Hindawi
International Journal of Optics
Volume 2017, Article ID 4750290, 12 pages
https://doi.org/10.1155/2017/4750290

Research Article

Research on Mud Flow Rate Measurement Method Based on Continuous Doppler Ultrasonic Wave

Quan Zhou,[1] Hui Zhao,[1] Yufa He,[2] Shengnan Li,[1] Shiquan Jiang,[2] and Huijie Zhang[3]

[1] *University of Electronic Science and Technology of China, Chengdu 611731, China*
[2] *CNOOC Research Institute, Beijing 100027, China*
[3] *Chengdu Technological University, Beijing 611000, China*

Correspondence should be addressed to Quan Zhou; quanzhou.uestc@gmail.com

Received 16 March 2017; Accepted 7 June 2017; Published 20 July 2017

Academic Editor: Giulio Cerullo

In deep-water drilling processes, the flow rate of drilling mud inside an annular pipe is significant judgment data for early kick detection. On the basis of the continuous-wave Doppler ultrasound, this paper proposes a new detection method of nonoriented continuous-wave Doppler ultrasound. The method solves the problem of the ultrasound having great attenuation in mud and not receiving effective signals by using a continuous ultrasound. Moreover, this method analyzes the nonoriented characteristics of ultrasound reflection on principle and proposes the detection of ultrasound Doppler frequency shift by detecting Lamb wave, which releases the detection of oil-based mud flow rate in a nonintrusive annular pipe. The feasibility of the method is verified through theoretical analysis and numerous experiments on a gas kick simulation platform. The measurement result has reached a flow accuracy approximating to the intrusive flow meter.

1. Overview

Early kick detection is an important method in preventing blowout accidents and plays a significant role in deep-water drilling processes. As an important judgment factor, emphasis is always placed on the flow detection of drilling mud in an annular pipe. However, the complicated nature of underwater environment and the detection of the mud flow that can only be conducted at the mud outlet cause serious hysteresis in gas kick detection results. The serious blowout accident that happened in the Gulf of Mexico, USA, in 2010 was greatly connected with the hysteresis in gas kick detection results. Knowing how to realize the detection of mud flow rate inside the annular pipe near the seabed and identifying the occurrence of the gas kick accident as early as possible are of great importance. However, two kinds of fluid flow detection methods exist: intrusive and nonintrusive. The intrusive flow meter will damage the original pipeline system and influence the drilling of the mud field, which makes the application of the intrusive method inevitably affect the original technological process. However, the deep-water drilling technology is complicated, and the requirement is high; thus, the change of the original technological process will bring about a cost increase. To have no influence on the original technological process, the best option is to have a nonintrusive flow detection method. Ultrasound flow detection is a typical nonintrusive flow detection method; however, mud drilling will cause ultrasound attenuation, and the common ultrasound detection method cannot detect effective echo signals. The continuous ultrasound will form a strong sound field in the mud and can spread further than the impulse ultrasound for the wave superposition factor. Nevertheless, few methods exist for detecting the flow rate of the continuous ultrasound. In addition, the measurement of the nonintrusive flow is difficult, because the flow mode of the annular pipe mud is complicated and the pressure at the seabed is remarkably high. On this basis, this study analyzes the nonoriented reflection of the continuous ultrasound in the drilling mud and establishes models. This work obtains the principle that part of the reflected ultrasonic waves transfer into Lamb waves when the reflection signal enters into a pipe wall from drilling muds. From these principles, the relationship between the reflection

signal frequency spectrum and flow rate can be obtained. The related flow rate detection algorithm finally solves the problem of the difficulty of applying ultrasound in deep-drilling flow detection.

2. Introduction

Numerous studies and applications of mud flow detection exist regarding early kick detection [1]. In 1987, Speers and Gehrig [2–4] proposed the calculation of exit and entrance flows to detect gas kick; flow detection with ultrasound can accurately measure mud flow and it is suitable for both water-based and oil-based mud. Furthermore, Orban et al. [2–4] measured the mud flow rate using the impulse generated by the return mud in the pipe, which is not only appropriate for different types of mud but also suitable for a large measurement range. Steine et al. [5] adopted the Coriolis flow meter in measuring mud flow and proposed the use of an electromagnetic flow meter to measure water-based drilling muds. However, these methods have been used to measure mud flow at the well head. Although they have great advantages in terms of accuracy and measurement, a large amount of rising gas will be relatively close to the well head when a large change of mud flow rate occurs at the well head and the time left for dealing with the accident is limited. After gas kick occurs, a multiphase flow will be formed by the combination of mud and methane gas. However, the measurements of the multi- and single-phase flows are not the same. Many researches started to analyze the multiphase flow detection. Wang et al. [6] used the DOP2000 ultrasound flow meter to research on the Doppler ultrasound characteristics, such as emission angle and attenuation; their research provides guidance for the reasonable application of the ultrasound flow meter. Obayashi et al. [7] used several probes to detect fluid comprehensively, which not only obtains fluid speed but also detects the flow direction of the fluid at different positions. Their method is significantly supportive for fluid-type judgment. In the experiments, all these methods have been used with water or oil. However, in an actual situation, the attenuation of ultrasound is large in drilling mud and increases along with the growth of mud density [8], which makes most methods inapplicable. To detect the occurrence of gas kick early, recent researchers have move towards the use of a downhole instrument, including the methods of pressure while drilling and logging while drilling [9]. Collett et al. [9] analyzed various parameters when gas kick occurs, such as flow, pressure, density, and electrical conductivity. The detection method at the downhole location has great advantages in terms of accuracy and stability. However, the layout of devices and equipment at the downhole will certainly increase the cost and technological complexity. For gas detection, the ideal mud flow detection position is at the mud line of the seabed. Therefore, Zhou et al. [10] proposed the use of ultrasound to detect mud flow. Fu et al. [11] conducted further research and several simulation experiments. The experiment result proved the feasibility of measuring mud flow using ultrasound. On this foundation, the current study analyzes and builds models for the principle of ultrasound reflection in drilling mud and explains the relationship between mud flow rate and Doppler frequency shift under the condition of continuous nonoriented ultrasound reflection.

The content of this paper is organized as follows. Section 3 describes the principle of the traditional Doppler flow meter. Section 4 presents the analysis of the principle of the nonoriented ultrasound reflection and the proposed flow rate detection method based on the nonoriented ultrasound reflection. Section 5 briefly describes the simulation platform, which is used in the experiments in Section 6. In Section 6, the experimental data and flow rate detection results are compared with the proposed method, and the target flow meter is described. The conclusion is presented in Section 7.

3. Theoretical Background

To provide a prompt and quick judgment reference for early kick detection, a flow detection device should be installed close to the probe. However, to keep the original structure of the annular pipe, only a nonintrusive flow detection method can be used. At present, the common nonintrusive flow detection methods are the flow detection methods based on ultrasound wave. Drilling mud contains a large number of fine particles, such as barite powder, and can be a solid–liquid–gas three-phase flow, which not only is remarkably complicated in the fluid type but also makes the ultrasound have a large attenuation inside. Therefore, the current normal ultrasound flow meters are inapplicable. To solve the problem, a set of ultrasound flow detection systems are designed based on the Doppler Effect. This method can be used to detect drilling mud in an annular pipe in deep-water drilling engineering and provide prompt flow data for early kick detection.

The Doppler Effect refers to the frequency change received by the observers for the relative movement between the wave source and the observers. A direct relationship exists between the change of frequency and the speed of relative movement. On this principle, the movement speed of the reflector can be detected through the change of the echo signal frequency reflected by the reflector in the detected fluid. For a steady fluid, the movement speed of the reflector can be roughly regarded as the overall movement speed of the fluid according to the fluid mechanics theory. The basic principle of the ultrasound flow meter is shown in Figure 1.

In Figure 1, β is the installation angle of the ultrasound sensor, φ is the refraction angle, c is the spread speed of ultrasound in fluid, v is the flow rate of fluid, c_1 is the spread speed of the ultrasound in acoustic wedge (coupling surface between sensor and pipe wall), and f_1 is the ultrasound frequency sent by the emission sensor. For the Doppler Effect, f_2 is the ultrasound frequency received by the moving particles in the fluid and f_3 is the ultrasound frequency received by the receiving sensor. The Doppler formula yields the following formula:

$$f_2 = f_1 \left(\frac{c \pm v_0 \cos \alpha}{c \mp v_s \cos \alpha} \right). \quad (1)$$

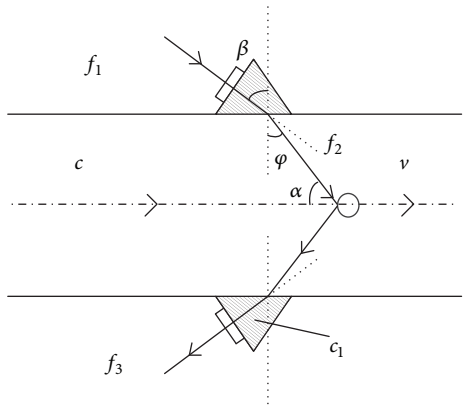

Figure 1: Basic principle of Doppler speed detection.

If the position of the emission source is fixed, then $v_s = 0$. According to the relative movement direction, the following formula is obtained:

$$f_2 = f_1 \frac{c - v\cos\alpha}{c}. \tag{2}$$

For the echo signal, if the position of the observer is fixed, then $v_0 = 0$. Thus,

$$f_3 = f_2 \frac{c}{c + v\cos\alpha}. \tag{3}$$

Combining (1) and (2) yields

$$f_3 = f_2 \frac{c}{c + v\cos\alpha}. \tag{4}$$

The Doppler frequency shift Δf is the difference between the emission frequency f_1 and the receiving frequency f_2. In drilling mud, the spread speed of the ultrasound is larger than 1500 m/s, which is significantly larger than the speed of drilling mud (usually <2 m/s). Therefore, the Doppler frequency shift Δf can be simplified as

$$\Delta f = f_1 - f_3 = f_1 \frac{2v\cos\alpha}{c}. \tag{5}$$

The flow rate is expressed as

$$v = \frac{c}{2f_1\cos\alpha}\Delta f. \tag{6}$$

According to Snell's principle, the relationship between the ultrasound angle of incidence and refraction angle is

$$\frac{\sin\beta}{\sin\varphi} = \frac{c_1}{c}, \tag{7}$$

$\sin\varphi = \cos\alpha$; thus,

$$\frac{c}{\cos\alpha} = \frac{c}{\sin\varphi} = \frac{c_1}{\sin\beta}. \tag{8}$$

Combining (8) with (6) yields the fluid flow rate, as shown as follows:

$$u = \frac{c_1}{2f_1\sin\beta}\Delta f. \tag{9}$$

If the acoustic wedge is solid, then the environment slightly influences the ultrasound spread speed. Meanwhile, the spread speed of the ultrasound in the drilling mud is easily impacted by the changes of several factors, including the density of drilling mud and temperature. In the formula above, the flow rate detection result has no connection with the spread of the ultrasound in the drilling mud; it is only connected with the frequency difference caused by mud speed and the spread of the ultrasound in the acoustic wedge. The fluid flow rate has greatly reduced the measurement error caused by the environment on principle. Therefore, it can be calculated using the detected Doppler frequency shift Δf.

In addition, given that the common Doppler ultrasound flow meter detects the average speed of the reflection particles in certain fluid areas, the area with the average fluid speed is connected with the Reynolds number of the fluid. Therefore, to detect the average speed of the overall fluid accurately, the common Doppler ultrasound flow meter usually introduces the flow rate correction system, which is the function between the Reynolds number and position parameter. First, for deep-water drilling, the fluid type in the drilling mud inside the annular pipe is not completely stable for the disturbance of the drill pipe and the complexity of the drilling process. Meanwhile, the impurities in mud, even the size, number, and distribution of bubbles, will change. Therefore, it is impossible to get the precise correction parameters before application. Second, a large number of fine particles exist in the drilling mud, and the attenuation of the ultrasound in the mud is great. Even if the area with an average flow rate can be identified, if the area is far from the emission and receiving areas, then the effective echo signal may not be received. Therefore, for deep-water drilling processes, a new ultrasound Doppler flow detection method is proposed in this study.

4. Nonoriented Continuous Doppler Ultrasound Flow Rate Detection

4.1. Principle of Nonoriented Continuous Doppler Ultrasound Flow Detection

4.1.1. Wave Mode Conversion. From the wave property, not only refraction and reflection but also wave mode conversion exists when the ultrasound enters into the interface of two different materials through oblique incidence with a certain angle, as shown in Figure 2.

Moreover, no transverse wave exists in the fluid. Thus, the spread speed of the longitudinal wave of the ultrasound in the drilling mud is c_L. The materials of the annular pipe and the ultrasound receiving acoustic wedge are rigid metal, so the velocities of the ultrasound in these two parts can be regarded as the same. c_{rL} is the spread speed of the longitudinal wave, c_{rS} is the spread speed of the transverse wave, the ultrasound

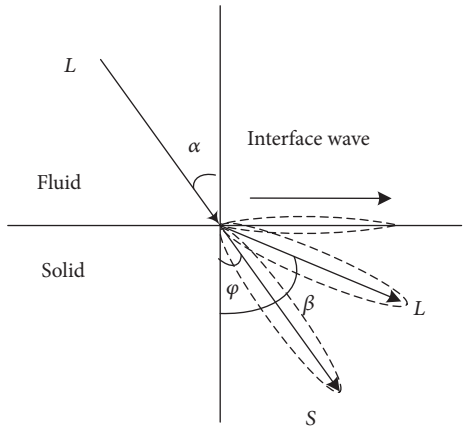

Figure 2: Refraction and wave mode conversion.

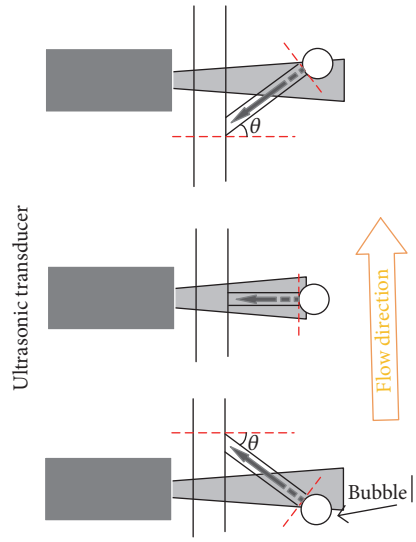

Figure 3: Different refraction angles in different positions.

that enters into the pipe wall from the drilling mud has angle α, β is the refraction angle of the longitudinal wave, and φ is the refraction angle of the transverse wave. Based on Snell's principle, the following formulas can be derived:

$$c_L \sin\beta = c_{rL} \sin\alpha, \tag{10}$$

$$c_L \sin\varphi = c_{rS} \sin\alpha. \tag{11}$$

If $\beta = \pi/2$ and $\varphi = \pi/2$, then the first and second critical angles are

$$\theta_L = \sin^{-1}\frac{c_L}{c_{rL}}, \tag{12}$$

$$\theta_S = \sin^{-1}\frac{c_L}{c_{rS}}. \tag{13}$$

According to the experimental measurement result, the spread speed of 64 K ultrasound in drilling mud with a density of 1.1 g/cm^3 is 1380 m/s, whereas that of the ultrasound longitudinal wave in the steel material is approximately 5850 m/s, and the f transverse wave is 3230 m/s. Therefore, according to (12) and (13), the first and second critical angles are calculated as $\theta_L \approx \pi/10$ and $\theta_S \approx \pi/5$, respectively. When the angle of incidence is larger than the first critical angle, all refraction longitudinal waves will transfer to the interface wave; when the angle of incidence is larger than the second critical angle, all the transverse waves, as well as the longitudinal wave, will transfer to the interface wave. The shape of the impurities of the drilling mud is different, and the position is random; thus, when the ultrasound spreads in the drilling mud, scattering phenomenon occurs and the signal reflected into the pipe wall enters with different angles. However, from the aforementioned calculation, the second critical angle is $\pi/5$, which implies that most of the incoming echo wave transfers to the interface wave.

4.1.2. The Model of Nonoriented Continuous-Wave Doppler. Based on (1), Doppler frequency shift can be expressed as follows:

$$f_d = \frac{2f_0 \sin\theta}{c} v. \tag{14}$$

If the fluid is steady, the velocity of ultrasonic reflectors is also steady. So, when an ultrasonic reflector with a regular shape passes through the ultrasonic field, the reflection angle should change continuously. The situation in which a bubble passes through the ultrasonic field is shown in Figure 3. The reflection angle θ is changed from $-\pi/2$ to $\pi/2$ continuously. So, the probability distribution of θ is uniform distribution:

$$f(\theta) = \frac{1}{\pi}, \quad -\frac{\pi}{2} < \theta < \frac{\pi}{2}. \tag{15}$$

Because f, c, and v are all constants in steady fluid, based on (14), the probability distribution of f_d is also uniform distribution:

$$f(f_d) = \frac{2f_0 v}{c} \sin\frac{1}{\pi}, \quad -\frac{2f_0 v}{c} < f_d < \frac{2f_0 v}{c}. \tag{16}$$

There are many reflectors in the ultrasonic field at the same time and their positions are different. So, θ could be positive and negative, and they are combined together at the same time so that it is hard to distinguish their directions. However, the flow direction in the annular pipe is known in deep-water drilling, so (16) can be simplified as (17) because of the symmetric property of θ:

$$f(f_d') = \frac{2f_0 v}{c} \sin\frac{2}{\pi}, \quad 0 < f_d < \frac{2f_0 v}{c}. \tag{17}$$

Assume that the distance from the pipe wall to the reflector is d (Figure 3); then, the distance of the reflected ultrasonic z is

$$z = \frac{d}{\cos\theta}, \quad 0 < \theta < \frac{\pi}{2}. \tag{18}$$

Based on attenuation property of sound waves, the amplitude of the reflected ultrasonic wave A_R can be calculated as

(19) if the original ultrasonic wave amplitude after reflecting is A_r:

$$A_R = A_r e^{-az} = A_r e^{-a(d/\cos\theta)}, \quad 0 < \theta < \frac{\pi}{2}. \tag{19}$$

A_r can be calculated in the same way. Assume that the original ultrasonic wave amplitude entering in fluid is A_0, the reflection coefficient is R, for any reflector i at time t, the distance from the pipe wall to the reflector i is d_i, the sectional area of ultrasonic field at positon d_i is S_{d_i}, the area for reflecting is S_i', and the total area of the reflector is S_i. Then, there is

$$A_{ri} = \frac{A_0 e^{-ad_i} R S_i'}{S_{d_i}}. \tag{20}$$

Combined with (19), the relationship between the original transmit ultrasonic signal and the received signal is as follows:

$$A_{Ri} = \frac{A_0 e^{-ad_i} R S_i'}{S_{d_i}} e^{-a(d_i/\cos\theta)}. \tag{21}$$

The attenuation of ultrasonic wave in mud is so high (usually >7 dB/cm when ultrasonic frequency is 500 KHz) that the maximum distance of the ultrasonic field is short. To simplify the model, the distribution of the positions of reflectors is assumed to be uniform distribution too:

$$f(i) = \frac{m}{S_{\text{unit}}}, \quad 0 < i < n, \ 0 \le m \le \frac{S_{d_i}}{S_i}. \tag{22}$$

In (22), S_{unit} is the unit area and m is the number of reflectors in the unit area. So, the total amplitude of the reflected ultrasonic wave A_R is the accumulation of A_{Ri} in every sectional area. A_R is shown in (23):

$$\begin{aligned} A_R &= \int_{d_i=0}^{z_r} A_{Ri} f(i) S_{d_i} d(d_i) \\ &= \int_{d_i=0}^{z_r} \frac{A_0 e^{-ad_i} R e^{-a(d_i/\cos\theta)}}{S_{d_i}} S_i' f(i) S_{d_i} d(d_i). \end{aligned} \tag{23}$$

In (23), z_r is the maximum distance of the ultrasonic field, $S_i' f(i) S_{d_i}$ means the total area of reflecting in the sectional area, and $\int_{d_i=0}^{z_r} S_i' f(i) S_{d_i} d(d_i)$ means the total volume of reflecting. If the shapes of reflectors are regular, the rate between the volume of reflecting and the total volume is constant. For example, if the shape of reflectors is spherical, the rate is equal to 1/2. k_s is used to represent the rate and it can be defined as $k_s = V_{Si}/V_i = \int_{d_i=0}^{z_r} (S_i'/S_i) d(d_i)$. Combined with void ratio $\varepsilon_G = V_G/V = \int_{d_i=0}^{z_r} (S_i f(i) S_{d_i}/S_{d_i}) d(d_i)$, (23) can be transformed as follows under the condition that the fluid is steady:

$$A_R = k_s \varepsilon_G A_0 R \int_{d_i=0}^{z_r} e^{-a(1+1/\cos\theta) d_i} d(d_i). \tag{24}$$

At some point, the ultrasonic field is settled and z_r is constant, so A_R will change with reflecting angle θ based on (9). Considering (14) and (21), when θ increases, the amplitude of the reflected ultrasonic wave decreases and the Doppler frequency shift increases for any reflector. The rate between the Doppler frequency shift and the amplitude of reflected ultrasonic wave is defined as follows:

$$\begin{aligned} a_f &= \frac{f_{di}}{A_{Ri}} = k_f \sin\theta e^{a(1+1/\cos\theta)}, \\ &0 < \theta < \frac{\pi}{2}, \ k_f = \frac{2\nu f_0}{c k_s \varepsilon_G A_0 R}. \end{aligned} \tag{25}$$

Based on (25), a higher Doppler frequency shift needs a larger weight coefficient to make sure that the result is accurate and the weight coefficients are related to the sine function.

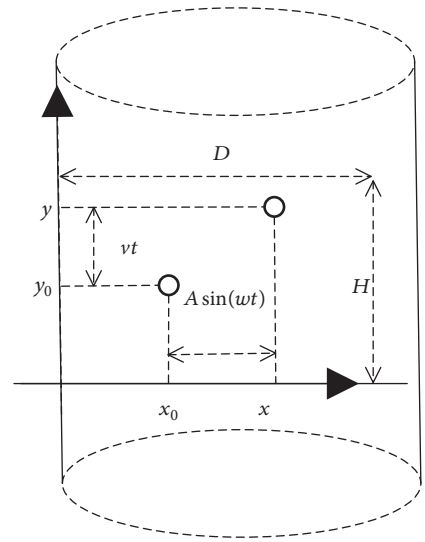

Figure 4: Simulation model.

4.1.3. Numeral Simulation of the Nonoriented Continuous-Wave Doppler Model. The spread angle is usually small when the frequency of the ultrasonic wave is high. In this paper, a 64 kHz ultrasonic wave is used and the spread angle is less than $\pi/18$ rad. To simplify the simulation model, the spread angle is ignored and the model is as shown in Figure 4. Assume that the depth of the ultrasonic field is D, the width is H, the original position of the reflector is (x_0, y_0), the velocity of the fluid is ν, the frequency of the reflectors' vibration on cross section is $\omega = 2\pi f$, and the maximum width of the vibration is A. Because positions of the reflectors are continuous, their updated position after time t can be expressed as follows:

$$\begin{aligned} x &= x_0 + A\sin(\omega t), \\ y &= y_0 + \nu t. \end{aligned} \tag{26}$$

Assume that the center of the ultrasonic sensor is $H/2$; then, the reflector angle can be calculated as follows:

$$\tan\theta = \frac{y - H/2}{x}. \tag{27}$$

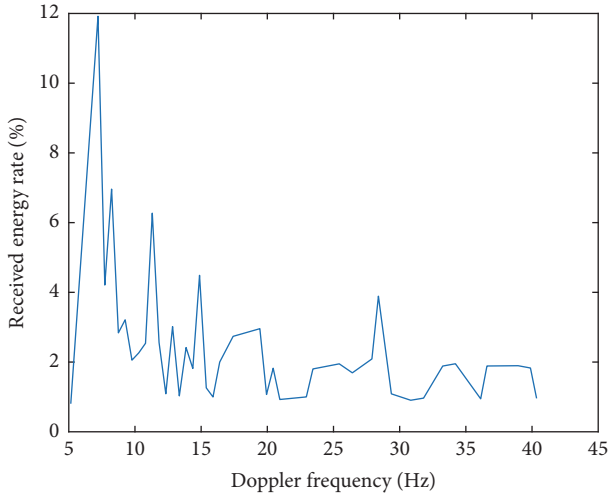

Figure 5: Simulation result when $N = 100$.

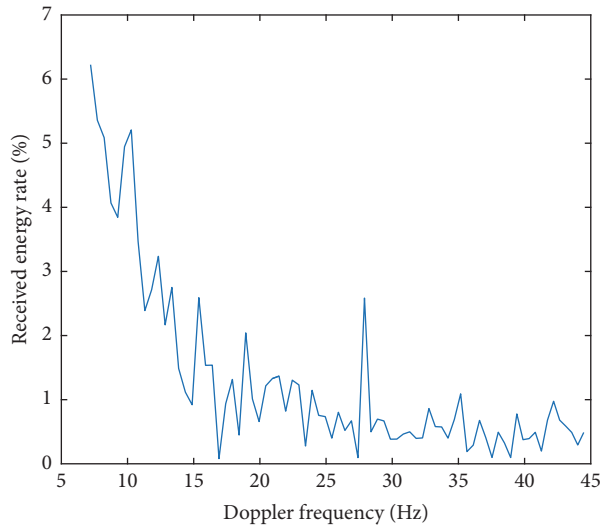

Figure 6: Simulation result when $N = 1000$.

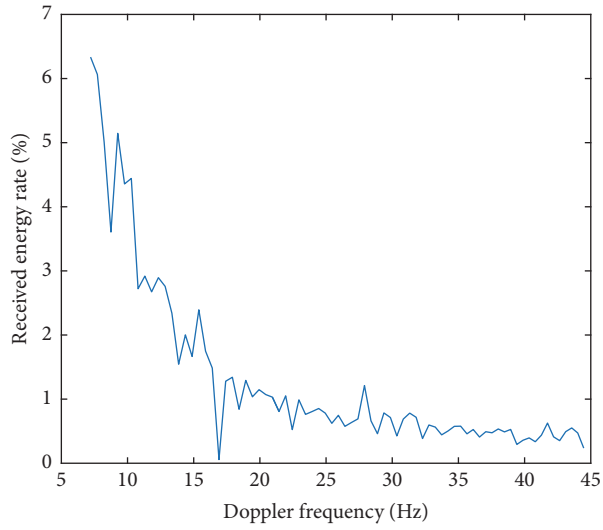

Figure 7: Simulation result when $N = 5000$.

Then, the power of the received ultrasonic signal and Doppler frequency can be calculated based on (19) and (14). Based on Figure 4, x_0 is random and y_0 is determined by the position at previous time. So, x_0 should be the parameters of the simulation model, y_0 should be assigned to 0 at the beginning, and the result needs to be calculated after $t_s = H/v$. The whole simulation process is as follows:

(1) Set simulation parameters: $v = 1$ m/s, $H = 0.05$ m, $D = 0.10$ m, $f_0 = 64$ kHz, $c = 1380$ m/s, $A = 0.01$, and $\omega = 2\pi$.

(2) Generate N random positions $(x_{01}, 0), (x_{02}, 0), \ldots, (x_{0N}, 0)$, which obey uniform distribution $U(0, D)$.

(3) Update all the reflectors' positions based on (26).

(4) Repeat Steps 2 and 3 in every $t_s/100$ seconds until $2t_s$.

(5) Find all the reflectors whose y are less than H, and then the Doppler frequency and the corresponding spectrum can be calculated based on (19), (14), and (27).

The simulation result is shown in Figures 5, 6, and 7 when $N = 100$, $N = 1000$, and $N = 5000$.

From the simulation result, there are two conclusions:

(1) The simulation results are in agreement with the proposed theory, which means the power of the lower Doppler frequency always occupies a large proportion.

(2) When N is smaller than 1000, the simulation results are unstable and this phenomenon is consistent with the statistical characteristics of the model.

4.1.4. Layout Design of the Overall Detection Devices. In wave refraction and wave shape transformation, the wave frequency will not be changed. Therefore, the flow rate can be detected using an ultrasonic receiving sensor with high sensitivity, considering the interface wave of the pipe wall as the echo wave signal. The overall plan is shown in Figure 8.

To solve the problem of the ultrasound wave having great attenuation in the drilling mud, a low-frequency ultrasound is selected, a set of high-power ultrasound driver devices are developed, and a continuous-wave-to-driver emission sensor is utilized. The emission end is mainly composed of the generation module, signal amplification module, ultrasonic driving module, and ultrasound emission sensor. Among them, the signal generation module can generate a 64 kHz sine wave signal continuously, which will be amplified by a signal amplifier; meanwhile, the driving emission sensor will generate a continuous ultrasound signal. The receiving part mainly comprises a signal amplification module, bandpass filter, mixer, acquisition card, and a PC. Among them, the signal amplification module will have linear amplification of the received weak echo signal and then the disturbance will be removed through the bandpass filter with a central frequency of 64 kHz. The function of the mixer is to compound the

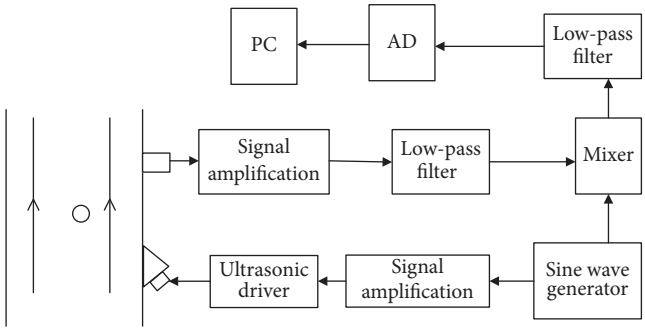

Figure 8: Layout design of the overall detection devices.

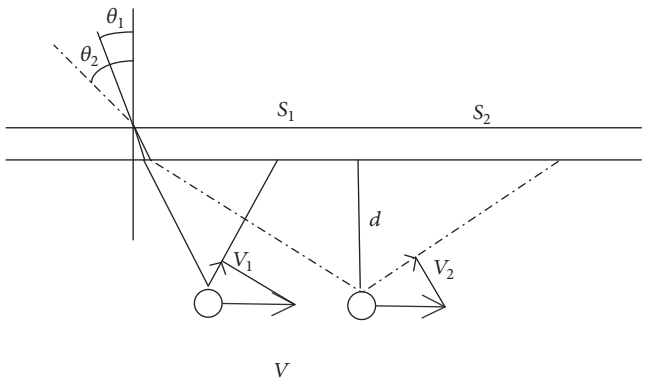

Figure 9: Influence of the reflection angle on measurement.

filtered and emitted signals into a compound signal with a frequency difference and a frequency sum. After entering into a low-pass filter with a cutoff frequency of 200 Hz, only the difference frequency signal will remain. Finally, after signal conditioning, the signal with Doppler frequency shift will be sent to a PC for storage and analysis by an A/D acquisition card (fs = 100 kHz).

4.2. Data Processing Algorithm for the Nonoriented Continuous Doppler Ultrasound Flow Detection. Doppler flow detection based on impulsive ultrasound can selectively deal with the echo signal reflected around the pipeline center through signal-receiving timing. However, for Doppler flow detection based on continuous ultrasound, the received signal is random due to the random position of the reflector in fluid, as well as the random reflection angle. Therefore, the traditional Doppler flow detection method cannot be used to process signals.

When the reflector moves at a constant speed (v_1, v_2) and generates two different echo wave signals (S_1, S_2) at two distinct positions, the Doppler frequency shift generated by speed is connected with the projection in the reflection direction, as shown in Figure 3. When the angle of reflection increases, the projection component becomes larger. According to the Doppler Effect, the frequency shift also increases. If the reflection angle increases, then the route will no longer be passed by the echo wave signal, as shown in Figure 9. In summary, if the angle of the reflection increases, then the difference of the echo ultrasound frequency increases, whereas the range of reflection signal decreases. Conversely, if the angle of reflection decreases, then the frequency difference decreases, whereas the range of reflection signal increases.

Aside from being influenced by the angle, the differences in Doppler frequency are distinct at different flow rates in different fluid areas. For example, for steady viscous fluid, the flow rate at the central position is larger than that around the pipe wall. However, for steady fluid, the distribution of the flow rate is stable in fluid. Therefore, theoretically, if enough sampling time is available, then the influence of flow rate in the different areas on the final result can be roughly ignored.

In the stable fluid, the reflector in the fluid often passes through the entire ultrasound emission sound field with the same speed (the scope of the sound field is connected with the diameter and frequency of the emission sensor). Thus, the emission angle is distributed evenly in the paper, and the length of the spread routine with the same distance but different angles is connected with the function. In the paper, weighting coefficients based on the sine function with a range of $[0, \pi/2]$ are used as a correction factor. The detailed algorithm steps are as follows:

(1) According to the actual fluid speed scope, the maximum frequency shift $f_{\max}$ is calculated.

(2) Based on $f_{\max}$, the digital low-pass filter is designed, the collected signal f is filtered, and the filtered signals are obtained as f'.

(3) The power spectrum P_i, $f_i \in (0, f_{\max})$, $i = 1, \ldots, n$, is obtained from signal f'-based SFFT. Based on (25), the result needs to be converted into dB form.

(4) When the flow rate is 0 m/s, the background noise power spectrum P_0 is obtained.

(5) According to the frequency scope of the power spectrum, the corresponding weighting coefficients a_i, $i = 1, \ldots, n$, are generated based on $\sin(0, \pi/2)$.

(6) The result is calculated as

$$\Delta f = \frac{\sum_1^n f_i a_i P_i'}{\sum_1^n a_i P_i'}, \quad P_i' = \begin{cases} 0, & P_i \le P_0 \\ P_i - P_0, & P_i > P_0 \end{cases} \tag{28}$$

to avoid noise influence on the final result.

(7) According to the large experimental data and flow meter data, the correction factors b_i can be obtained, and the flow rate measure can be applied under the same experimental condition.

Formula (6), instead of (9), is used in the calculation in Step 1 because of the reflection angles and the distinct position and shape of the reflectors, but not related to the emission angle. Therefore, the largest frequency shift is the one with the maximum flow rate, as expressed in the formula

$$f_{\max} = \frac{2u_{\max} f_1}{c}. \tag{29}$$

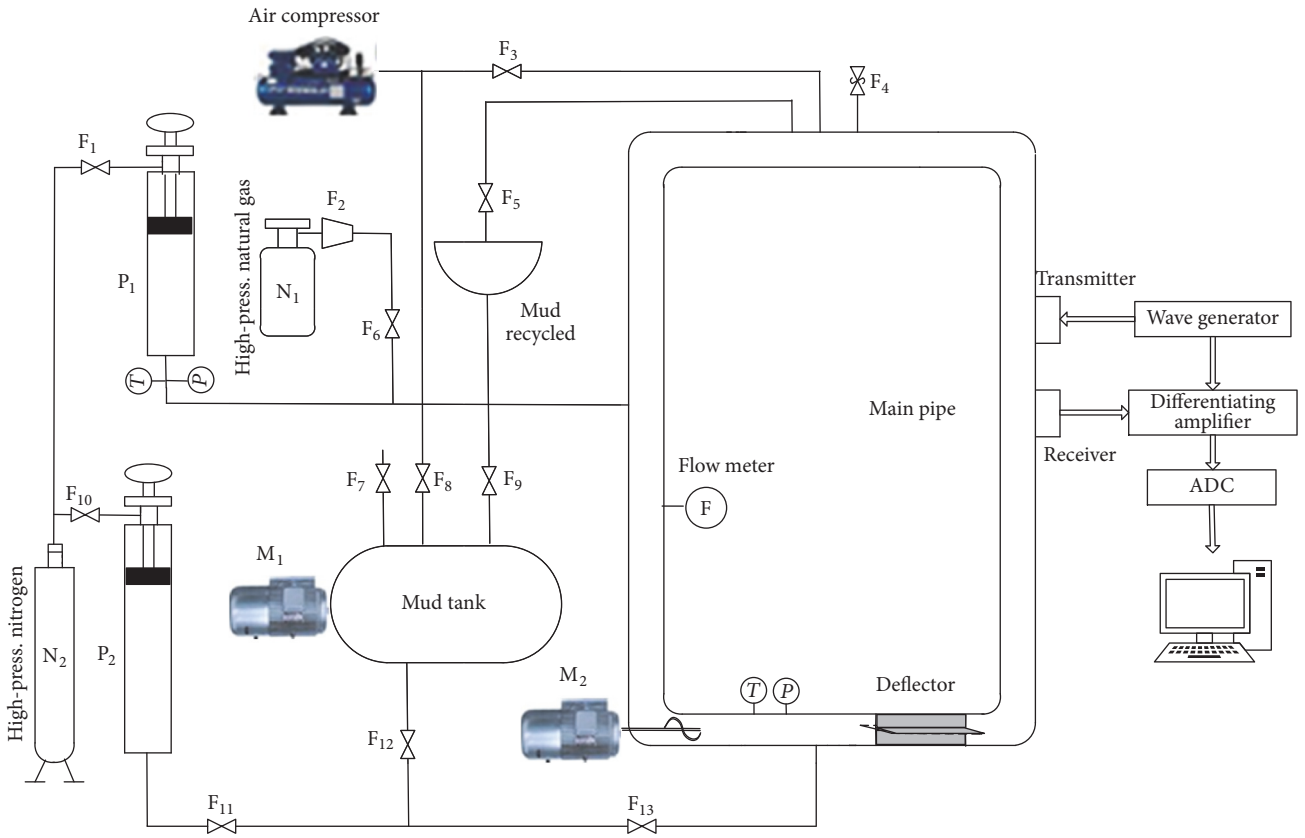

Figure 10: Schematic diagram of the experimental platform.

5. Experiment Devices and Steps

The experimental platform of deep-water drilling gas kick detection is mainly composed of a main circulation pipe, mud injection device, natural gas injection and pressure device, cycle pump, and detection device, as shown in Figure 10. Among the parts mentioned, the main pipe is a pressure steelwork circular tube, which is the main place for the mixing and flowing of mud and natural gas. The main pipe has an inner diameter of 200 mm, height of 3.4 m, and width of 1.4 m. The integrated mud pump can prompt a circulation flow of mud in the pipe. Meanwhile, the intrusive flow meter, safety valve, pressure meter, and thermometer installed on the pipe can measure the related parameters of the pipe fluid. The mud injection device contains a mud agitator, mud tank, and air compressor. By using the air compressor to add pressure for the mud tank, the mud can be pressed into the main circulation pipe. When the injected mud enters into the recycle device, then the mud is sufficient. The natural air injection and pressure device mainly consists of a natural gas tank, high-pressure nitrogen gas, and a piston. Among them, the high-pressure nitrogen tank is a pressuring device, which can prompt the piston to inject the natural gas into the circulation pipe and prompt the piston to squeeze the mud to add pressure for the entire pipe. The entire experimental platform principle is shown in Figure 10, and the actual experimental device is shown in Figure 11.

Figure 11: Experimental platform of the deep-water drilling gas kick.

Given that the frequency of the ultrasound is low and the solid particle in pure mud is also small, obtaining an effective reflection signal is difficult. In the experiment, adding a small

amount of natural gas can create a void fraction rate of around 3%. Then, mixing the gas into the moving mud can effectively measure the mud flow rate. The detailed steps are as follows:

(1) In the mud mixer, the drilling mud is stirred completely and then injected into the mud tank through F_1. Then, F_1 is closed, and F_2, F_4, and F_5 are opened. The air compressor presses the mud into the main circulation pipe until some mud enters into the mud recycle device.

(2) All valves are closed, and natural gas is injected in piston P1. Then, F_3, F_6, F_8, and F_9 are opened, and P1 is prompted to press the natural gas into the main circulation pipe through high-pressure nitrogen gas; meanwhile, the mud total volume V can be calculated through piston P2. The void fraction rate and the total volume of the main body of the circulation pipe can be calculated through V. When the void fraction rate reaches 3%, all the valves are closed, and gas injection is stopped.

(3) The mud pump is opened, and the mud pump rotation speed is adjusted through the transducer that indirectly controls the fluid speed in the main body of the circulation pipe.

(4) The actual fluid flow rate is read using the intrusive flow meter. When the flow rate is stable, the detection device can be used to measure fluid flow and speed.

(5) By repeating Steps 3 and 4, the detection data with different flow rates can be obtained.

6. Experiment Data and Verification

In the experiment, when the transducer is at a maximum of 50 Hz, the maximum flow rate by the flow meter is 1.0 m/s. The moving speed of the particles at the high flow rate area is assumed to be 1.5 times the average flow rate to have a sufficient margin. Meanwhile, the spread speed of the ultrasound in the mud is $c = 1320$ m/s and $f_1 = 64$ kHz; the maximum flow rate is 1 m/s according to (14); and $f_{\max} = 2uf_1/c \approx 145$ Hz. In the experiment, the data acquisition card used is Advantech PCI-1714UL. By using the Matlab driving acquisition card, the detection signal data can be sampled with 100 kHz sampling frequency, 10-bit depth, and an amplitude scope from −5 V to 5 V. In the experiment, oil-based drilling mud is adopted with a density of 1.1 g/cm^3; the added natural gas creates a void fraction rate of approximately 3%; the pressure in the main circulation pipe is 0.8 MPa; and the environment temperature is 27°C. After the motor has been operated for a while, the temperature will rise and the maximum temperature can reach 35°C given the friction inside the fluid and the heating of the mud pump. After ten groups of experiments, several sets of data can be collected for analysis. Some sampling results are shown in Figures 12–18. Among the figures, the upper-half part is the wave shape of the detection signal in the time domain, and the lower-half part is the related power spectrum; the frequency scope is below 150 Hz.

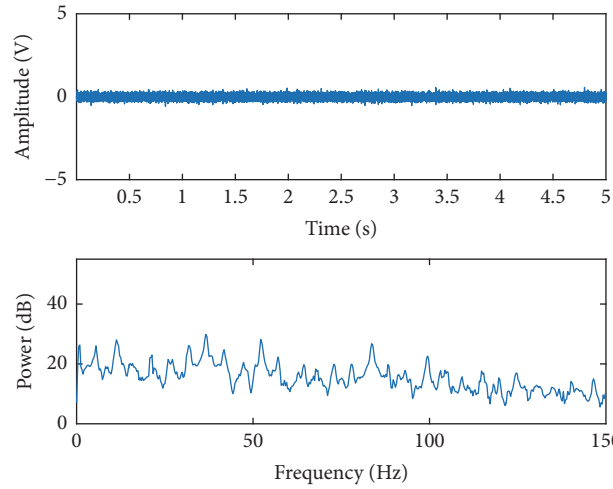

Figure 12: Received signal and power spectrum when the transducer frequency is 5 Hz and flow meter value is 0.13 m/s, in the absence of bubbles.

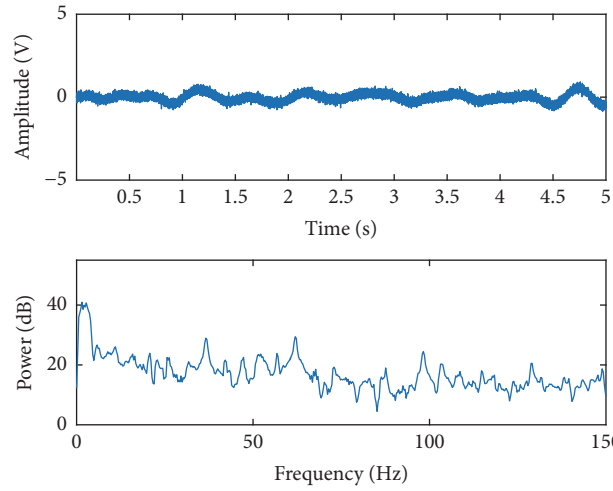

Figure 13: Received signal and power spectrum when the transducer frequency is 5 Hz and flow meter value is 0.15 m/s, in the presence of bubbles.

The measurement results when the frequency of the transducer is 5 Hz and the intrusive flow meter value is 0.13 m/s are shown in Figure 12; however, the detected signal is obviously a background noise. When the transducer frequency is 5 Hz, the thrust generated by the mud pump is small; thus, the overall flow rate of the mud is also small. However, natural gas bubbles are concentrated at the top of the main body of the circulation pipe. Mixing the bubbles into the mud circulation is difficult; thus, no bubbles pass by the detection pipe and no effective reflection signal can be detected. To solve this problem, the transducer can be adjusted to the maximum 50 Hz, which enables the mud flow rate to reach the maximum and complete the mixing of mud and natural gas. After being stable for a period of time (more than 30 s), the transducer frequency can be adjusted to 5 Hz,

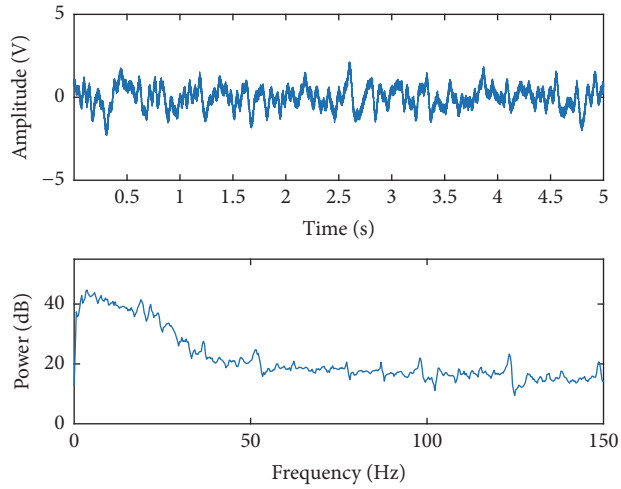

Figure 14: Received signal and power spectrum when the transducer frequency is 20 Hz and flow meter value is 0.36 m/s.

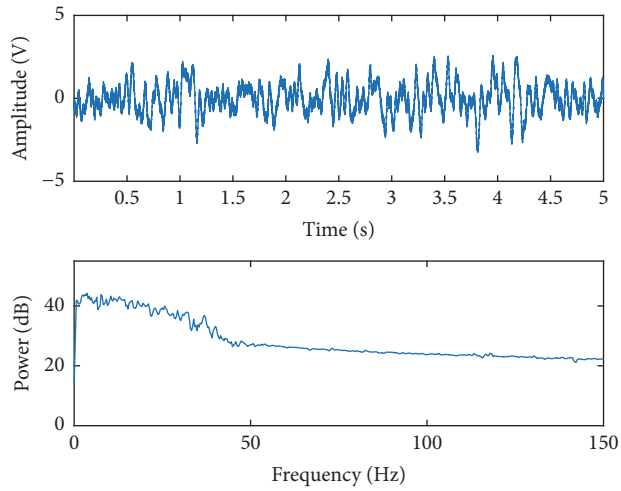

Figure 15: Flow meter value is 0.49 m/s when the transducer frequency is 25 Hz.

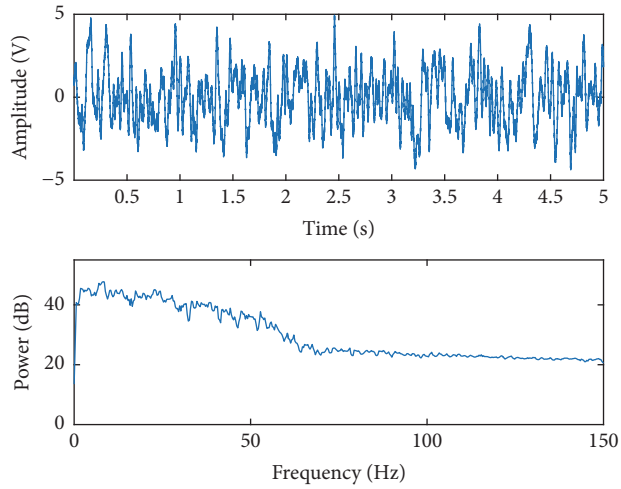

Figure 16: Received signal and power spectrum when the transducer frequency is 35 Hz and flow meter value is 0.71 m/s.

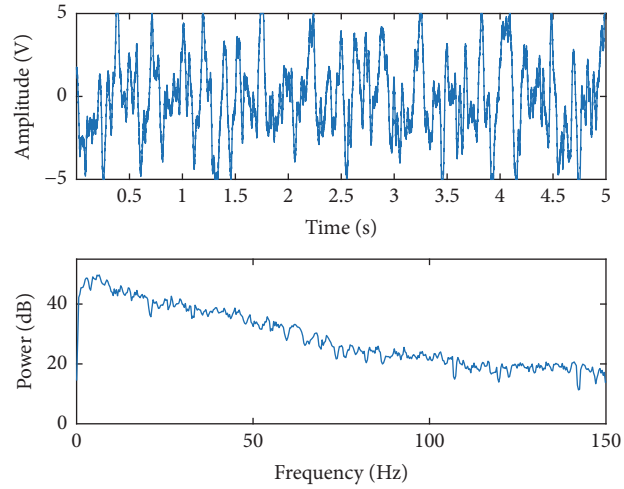

Figure 17: Received signal and power spectrum when the transducer frequency is 45 Hz and flow meter value is 0.86 m/s.

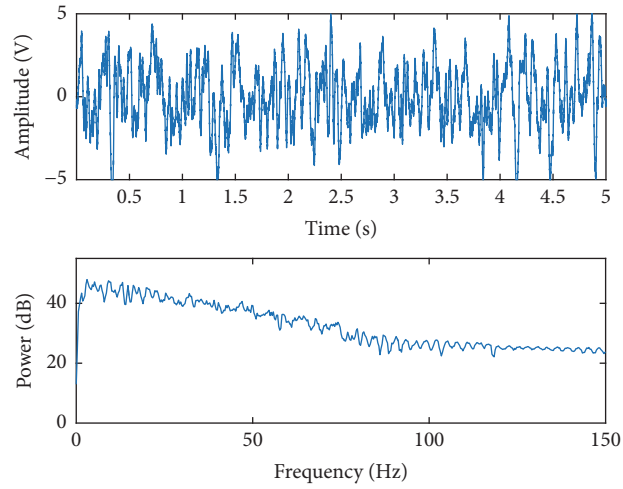

Figure 18: Received signal and power spectrum when the transducer frequency is 50 Hz and flow meter value is 0.96 m/s.

and detection is conducted when the flow meter is stable. The result is shown in Figure 13.

Either from the time domain or from the frequency signal, the high-frequency component increases gradually with the increase of mud flow rate, as shown in Figures 12–16. This result verifies the influence of the reflection angle on the detection signal and the accuracy of the proposed flow rate detection method. The detection signal and the frequency spectrum when the frequency of the transducer is 50 Hz are shown in Figure 16; no difference exists between the detection signals at 50 Hz and 45 Hz. In fact, the reading of the intrusive flow meter is unstable. When the frequency is above 40 Hz, the fluctuation scope of the flow rate measurement reaches ±0.2 m/s. The fluid inside cannot be directly observed since the mud is not transparent. However, given the instability of slow speed, the fluid may not be stable. Thus, the measurement error scope is large, and data measurement is now significantly random and unstable. Therefore, in the

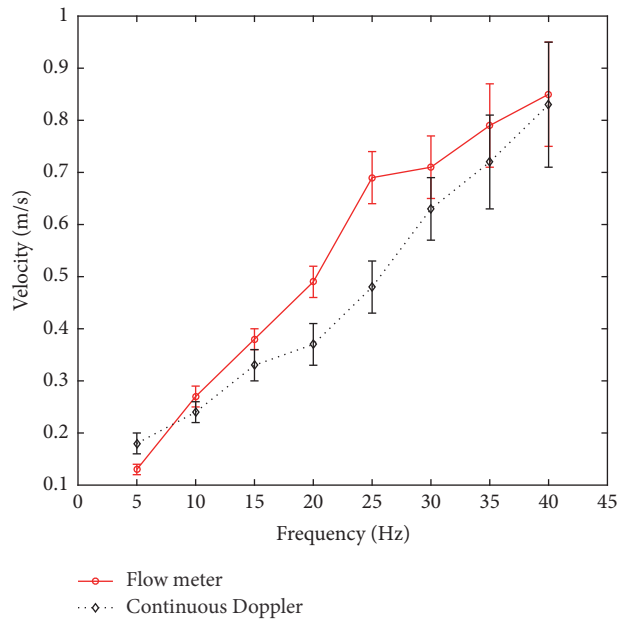

Figure 19: Comparison between the proposed method and the target flow meter.

final correction of the flow rate, the part with the transducer frequency above 40 Hz is not included in the calculation.

From the 10 experimental groups, the frequency has been adjusted from 5 Hz to 50 Hz in each group and then returns to 5 Hz with an interval of 5 Hz, thereby obtaining 20 groups of measurement data. As shown, Figure 19 shows that the proposed algorithm processes data and compares the result with the target flow meter readings.

According to the detection result, when the flow rate is small, the error scope is limited no matter how it is calculated through the continuous Doppler method or target flow meter reading. Meanwhile, the error range increases with the increase of flow rate. When the flow rate reaches 0.8 m/s, the error scope is approximately 0.1 m/s; when the flow rate is slow, the absolute error of measurement result is approximately 0.01 m/s, and the relative error is small. Although the error scope of the overall measurement result is large, it is in the same trend with the measurement result of the target flow meter. After more than ten groups of experiments and parameter corrections, a rather correct measurement can be obtained.

7. Conclusion

This paper proposes the nonintrusive flow rate measurement targeting for drilling mud in a deep-water drilling annular pipe. The proposed method solves the problem of difficulty in obtaining measurement due to the great attenuation of ultrasound in mud. Based on the continuous nonoriented Doppler ultrasound, the proposed method obtains an effective ultrasound reflection signal by collecting Lamb wave after wave mode conversion and obtains a related flow rate algorithm through the even distribution characteristics of the reflection angles. A few experiments show that the proposed method can be used to measure oil-based mud flow rate in the annular pipe and is consistent with the theoretical analysis. Although the accuracy of the method is relatively lower than the target flow meter, it has greater advantages in deep-water drilling gas kick area for its nonintrusive characteristics. The proposed method can measure mud flow rate in deep-water mud line annular pipes without damage on the original drilling technology and process. The application of the method can provide more prompt mud flow information and change compared with the current gas kick detection at the well head. This result can greatly advance the prewarning of the gas kick alarm and avoid occurrence of gas kick, even during a blowout accident. However, some shortcomings still exist in the current study. The detection accuracy is not sufficiently high; thus, the detection result shall be calibrated in advance in different environments. Moreover, the experiment device has not verified the detection situation when flow rate is larger than 0.8 m/s. In future works, the principal model shall be improved, and the method shall be verified and optimized with a better experiment platform.

Conflicts of Interest

The authors declare that they have no conflicts of interest.

Acknowledgments

This work is supported by the National Science and Technology Major Project of the Ministry of Science and Technology of the People's Republic of China (no. 2011ZX05026-001).

References

[1] D. Fraser, R. Lindley, D. D. Moore, and M. V. Staak, "Early Kick Detection Methods and Technologies," in *Proceedings of the SPE Annual Technical Conference and Exhibition*, Society of Petroleum Engineers, Amsterdam, The Netherlands, October 2014.

[2] J. J. Orban and K. J. Zanker, "Accurate flow-out measurements for kick detection, actual response to controlled gas influxes," in *Proceedings of the SPE/IADC Drilling Conference*, Society of Petroleum Engineers, 1988.

[3] J. M. Speers and G. F. Gehrig, "Delta flow: an accurate, reliable system for detecting kicks and loss of circulation during drilling," *SPE Drilling Engineering*, vol. 4, no. 2, pp. 359–363, 1987.

[4] D. Schafer, G. Loeppke, D. Glowka, D. Scott, and E. K. Wright, "An evaluation of flowmeters for the detection of kicks and lost circulation during drilling," in *Proceedings of the SPE/IADC Drilling Conference*, Society of Petroleum Engineers, New Orleans, Louisiana, 1992.

[5] O. G. Steine, R. Rommetveit, and T. W. R. Harris, "Full scale kick detection system testing relevant for slim-hole/HPHT drilling," in *Proceedings of the 1995 SPE Annual Technical Conference and Exhibition*, October 1995.

[6] T. Wang, J. Wang, F. Ren, and Y. Jin, "Application of Dopper ultrasound velocimetry in multiphase flow," *Chemical Engineering Journal*, vol. 92, no. 1-3, pp. 111–122, 2003.

[7] H. Obayashi, Y. Tasaka, S. Kon, and Y. Takeda, "Velocity vector profile measurement using multiple ultrasonic transducers,"

Flow Measurement and Instrumentation, vol. 19, no. 3-4, pp. 189–195, 2008.

[8] A. J. Hayman, "Ultrasonic properties of oil-well drilling muds," in *Proceedings of the Proceedings., IEEE Ultrasonics Symposium*, IEEE, Montreal, Quebec, Canada, 1989.

[9] T. S. Collett, M. W. Lee, M. V. Zyrianova et al., "Gulf of mexico gas hydrate joint industry project leg II logging-while-drilling data acquisition and analysis," *Marine and Petroleum Geology*, vol. 34, no. 1, pp. 41–61, 2012.

[10] Q. Zhou, H. Zhao, H. Zhan, H. Zhang, and C. Lu, "The application of ultrasonic based on Doppler effect used in early kick detection for deep water drilling," in *Proceedings of the 2013 International Conference on Communications, Circuits and Systems, ICCCAS 2013*, pp. 488–491, November 2013.

[11] J. Fu, Y. Su, W. Jiang, and L. Xu, "Development and testing of kick detection system at mud line in deepwater drilling," *Journal of Petroleum Science and Engineering*, vol. 135, pp. 452–460, 2015.